Chapter 7

Advances in Electrochemical Nitric Oxide Exhaust Gas Sensors

Erica Perry Murray and Ling Cui

Additional information is available at the end of the chapter

http://dx.doi.org/10.5772/62625

Abstract

The role of porosity on impedancemetric NO_x sensing is discussed for sensors composed of a porous yttria-stabilized zirconia (YSZ) electrolyte and dense Au electrodes. NO_x sensors considered here were fabricated at firing temperatures of 950–1200°C, which established a range of electrolyte microstructures where the porosity ranged from approximately 50% to 44%. Analysis of the electrical response of the NO_x sensors indicated that sensors fired at 1050°C resulting in an electrolyte porosity of 46% demonstrated higher NO_x sensitivity based on the operating conditions studied. The impedance of the sensors demonstrated a strong dependence on the electrolyte porosity. The activation energy of the sensors, which ranged from 109.2 to 81.1 kJ/mol, decreased with decreasing electrolyte porosity. Sensors with an electrolyte porosity ≥46% were limited by dissociated adsorption, whereas gas diffusion was rate limiting for sensors with an electrolyte porosity <46%. The impedancemetric response of the porous sensors to NO concentrations ≤10 ppm was distinguishable at operating frequencies as high as 40 Hz, thereby suggesting rapid sensing capabilities. Overall, the microstructure of the sensors composed of a YSZ electrolyte with 46% porosity promoted a strong, rapid, and highly sensitive response to NO_x.

Keywords: NO_x sensors, porous zirconia, impedancemetric, impedance spectroscopy, dense Au electrodes

1. Introduction

Automotive exhaust gas sensors play a critical role in monitoring emission components, such as nitric oxides, carbon monoxide, and hydrocarbons. These sensors also communicate with the vehicle on-board diagnostic system in order to regulate engine operation. Environmental

regulations have largely been responsible for driving improvements in gasoline and diesel engine operation and efficiency, as well as the use of cleaner fuels, which have translated into lower pollutant levels [1–3]. Monitoring lower pollutant levels requires the application of sensors capable of detecting exhaust gas constituents with greater sensitivity, selectivity, and accuracy.

Nitric oxides (NO and NO_2), referred to as NO_x, are highly regulated exhaust gas species as these emissions significantly contribute to environmental and respiratory health issues. Vehicles with diesel engines tend to emit higher concentrations of NO_x emissions, in comparison to vehicles using gasoline engines. Thus, NO_x sensors are a crucial component in diesel exhaust aftertreatment systems. Ceramic oxide-based electrochemical sensors are widely used as NO_x sensors as they can rapidly respond to changes in the exhaust gas composition. Traditionally, these sensors have utilized a dense zirconia-based electrolyte accompanied by porous noble metal electrodes. The porous electrodes allow the exhaust gas to diffuse to reaction sites along the electrolyte/electrode interface within the sensor. This interface is called the triple-phase-boundary (TPB). As the exhaust gas diffuses, it is possible for heterogeneous catalysis reactions involving NO_x to occur within the electrodes, thereby, resulting in a lower concentration of NO_x at the TPB. This can be particularly problematic for accurately detecting low concentrations of NO and NO_2 gases. Current NO_x sensors can accurately detect NO_x concentrations down to approximately 10 parts per million (ppm). Martin et al and Ling et al [4, 5] have found that greater sensitivity can be achieved by changing the microstructure of sensor components, such that the electrolyte is porous and the electrodes are dense. Using this sensor architecture, which is opposite to conventional NO_x sensors, has enabled NO and NO_2 to be detected at concentrations as low as 5 ppm. The dense electrodes seem to limit heterogeneous catalysis reactions, while the porous electrolyte allows NO_x gases to proceed to the TPB where NO_x sensing reactions occur. The degree of porosity within the electrolyte, as well as the morphology, significantly influences the exhaust gas diffusion path, diffusion rate, and concentration of reaction sites at the TPB. Thus, in order to gain greater understanding of porous electrolyte properties that influence the electrochemical response of NO_x sensors it is necessary to understand the behavior of a broad range of electrolyte microstructures.

This chapter concentrates on the behavior of NO_x sensors composed of a porous yttria-stabilized zirconia (YSZ) electrolyte. YSZ is favored as the electrolyte in NO_x sensors due to its tolerance for both lean and rich exhaust gas conditions [6]. Under lean exhaust conditions, the oxygen concentration in the exhaust is high, whereas rich conditions create an oxygen-reducing environment. The yttria content contributes to the mechanical and ionic properties of the material. Fully-stabilized zirconia (i.e., 8 mol% Y_2O_3-stabilized ZrO_2) has a reasonably high ionic conductivity, which contributes to the magnitude of the NO_x sensitivity response [7]. The pores of the YSZ electrolyte provide pathways for gas diffusion, while the contiguous network of YSZ particles provides pathways for ionic transport. These pathways are dependent upon the electrolyte microstructure.

The various electrolyte microstructures presented in this chapter were studied using the impedancemetric method for NO_x sensor operation. Impedancemetric NO_x sensing is a relatively new approach that is favored for the potential to overcome performance limitations associated with other methods; and, lower manufacturing costs are expected to be more readily

http://dx.doi.org/10.5772/62625

achieved by using this approach [4]. The following discussion will address the role of the NO_x sensor electrolyte microstructure, in terms of porosity, particle size, particle-to-particle contact, and TPB reactions, based on analysis of impedancemetric NO_x sensing for various operating conditions.

2. Impedance theory

Electrochemical impedance spectroscopy is a valuable and commonly used technique for examining the dynamics of mobile and bound charges within the bulk or at the interface of solid and liquid materials [8]. It is useful for investigating the electrochemical behavior of NO_x sensors, and can provide an understanding of the dependent relationship between NO_x reactions, and the composition, microstructure, and configuration of materials composing the sensor. Analysis of impedance data can also indicate potential reaction steps, such as adsorption, dissociation, diffusion, charge transfer, and ionic transport that can promote or limit the electrochemical behavior of the sensor. The impedance, Z, of a material is obtained by applying a small alternating voltage or current to the material sample and measuring the electrical response with respect to frequency, f. The impedance describes the opposition to current flow not only due to resistance, but also from capacitance and inductance effects that vary with frequency. The impedance is generally described in the complex plane by the real component, $Re(Z)$, and the imaginary component, $Im(Z)$, according to the following equations:

$$Z(\omega) = Re(Z) + jIm(Z) \tag{1}$$

where $\omega = 2\pi f$

$$Re(Z) = |Z|cos\theta \tag{2}$$

$$Im(Z) = |Z|sin\theta \tag{3}$$

The magnitude $|Z|$ is:

$$|Z| = \sqrt{\left[Re(Z)\right]^2 + \left[Im(Z)\right]^2} \tag{4}$$

and the phase angle, θ, is given by,

$$\theta = \tan^{-1}\frac{Im(Z)}{Re(Z)} \tag{5}$$

$|Z|$ or θ is commonly used to quantify the NO_x sensing response by the impedancemetric method. Some studies have found the θ response yields more sensitive and stable data in comparison to the $|Z|$ response [4]. For both $|Z|$ and θ, the sensing signal is frequency dependent, such that it is necessary to determine an appropriate frequency that enables noise factors to be minimized and the sampling rate to be maximized. Such conditions contribute to sensor accuracy, as well as a rapid response.

3. Experimental

Standard ceramic processing methods were used to fabricate NO_x sensors with a range of porous electrolyte microstructures. Tape cast 8 mol% Y_2O_3-stabilized ZrO_2 (YSZ, Tosoh Corp.) was used for the electrolyte along with gold (Au) wires that served as dense electrodes. The tapes were made by mixing YSZ powder with ethanol, binder (B-98 Butvar), dispersant (phosphate ester), and plasticizer (dipropylene glycol benzoate). The mixture was ball milled, dried, tape cast, and subsequently cut into rectangular strips that were approximately 10 mm × 5 mm × 1.5 mm. Further details concerning the fabrication steps are described elsewhere [5]. A YSZ slurry was made by dissolving additional YSZ tape into ethanol. This slurry was used to adhere layers of tape and coat the Au wire electrodes composing the NO_x sensors. One of the Au wire electrodes was wrapped outside of the assembly and the other Au wire was embedded between the YSZ tape layers. Additional YSZ slurry was coated over the entire sensor assembly. Illustrations of similar sensors were published by Cui and Murray [9]. The sensors were fired in air at 950, 1000, 1050, 1100, 1150, and 1200°C for 1 hour. The different firing temperatures resulted in different porous electrolyte microstructures and morphologies. Scanning electron microscopy (SEM) combined with statistical calculations and Archimedes method were used to analyze the porosity of the electrolytes. The statistical approach and calculations are discussed in reference [5].

Impedancemetric operation of the NO_x sensors was carried out using a Gamry Reference 600 that was set to apply a small alternating voltage of 50 mV across the sensor and record the electrochemical response over frequencies ranging from 1 Hz to 1 MHz. Experiments took place in a quartz tube within a furnace operated at temperatures of 600–700°C. A standard gas handling system composed of mass flow controllers was used to manage the supply of exhaust gas mixtures containing O_2, N_2, NO, and NO_2 for a total flow rate of 100 sccm. This flow rate was chosen to allow sufficient time for the gases to adsorb and diffuse through the pores within the electrolyte to the electrolyte/electrode interface. NO and NO_2 concentrations up to 100 ppm were studied with particular focus at lower concentrations (i.e., <20 ppm). These measurements were collected in the presence of 1% to 18% O_2 with N_2 as the balance gas. The phase angle component of the impedance, θ, was used to determine the sensitivity to NO and NO_2. Equivalent circuit analysis was used to model the impedance data in order to interpret

http://dx.doi.org/10.5772/62625

activation energies, oxygen dependence, and potential rate limiting mechanisms impacting the NO_x sensing response.

4. Electrolyte microstructure and morphology

Typical SEM images of the various porous YSZ electrolytes fired at temperatures ranging from 950°C to 1200°C are shown in **Figure 1**. These images show the surface of the NO_x sensor electrolyte. The cross-sectional images (not shown) were very similar to the corresponding surface images. For sensors fired at lower temperatures, the YSZ particles were smaller in size and there was less contact between particles, in comparison to the electrolyte for sensors fired at higher temperatures. The SEM images showed YSZ particles of similar size, ranging from approximately 60 to 80 nm, for firing temperatures up to 1050°C. At 1100°C, there was a noticeable change in the microstructure as greater necking was observed between connected particles. As the firing temperature increased, the porous pathways and network of electrolyte particles became more distinct. Surface cracks were observed on electrolytes fired at 1150 and 1200°C. These defects were more substantial in electrolytes fired at 1200°C, which may indicate that thermal stresses were the source.

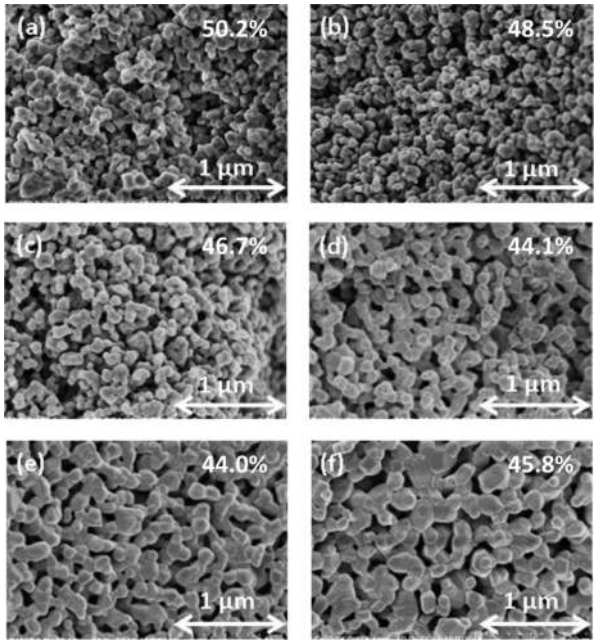

Figure 1. SEM images of YSZ electrolytes fabricated at (a) 950°C, (b) 1000°C, (c) 1050°C, (d) 1100°C, (e) 1150°C, and (f) 1200°C.

The porosity was calculated using a three-dimensional statistical method based on the difference in contrast between the pores and particles shown in the SEM images of the YSZ electrolytes. **Table 1** shows the porosity values determined for each sensor. The porosity decreased by about 6% for sensors fired between 950 and 1100°C. However, only a small change in porosity was observed for sensors fired at 1100 and 1150°C; and, an unexpected increase in electrolyte porosity was determined for sensors fired at 1200°C. It is likely that the cracks observed in the sensors fired at 1150 and 1200°C were a source of error in this data. Porosity measurements by Archimedes method, also shown in **Table 1**, were found to decrease with increasing firing temperature, and were consistently about 6% higher than the porosity calculations by the statistical method. Using Archimedes method, open pores composing the entire YSZ electrolyte were accounted for in the measurement; whereas the statistical method was based on a series of surface images of the electrolyte. Although Archimedes method is more prone to human error, it is possible that more reliable data, particularly for the electrolytes with surface cracks, are depicted in the results from Archimedes method.

T_f (°C)	Mathematical method		Archimedes method	
	Porosity (%)	σ (%)	Porosity (%)	σ (%)
950	50.16	1.82	56.6	0.87
1000	48.54	2.21	55.5	0.85
1050	46.70	1.88	52.3	1.11
1100	44.10	0.87	51.1	1.15
1150	44.06	0.66	50.6	0.64
1200	45.80	0.78	43.9	0.62

Table 1. Porosity results from mathematical method and Archimedes method as a function of the YSZ electrolyte fabrication temperature, T_f.

5. Impedancemetric NO_x response

The impedancemetric response of the various sensors to NO_x indicated similar data for the response to NO and NO_2. This is a common observation that has been associated with thermodynamic conversion of NO_2 to NO at elevated temperatures [5, 10]. Given this observation, representative data collected for NO are presented. Typical impedance data collected for the sensors indicated a strong relationship between the sensor electrolyte fabrication temperature and the magnitude of the impedance response. This can be seen in the impedance data collected for sensors with electrolytes fired at 1000, 1100, and 1200°C that were operated at 650°C in the presence of 10.5% O_2, shown in **Figure 2**. The data were measured in triplicate for each testing condition to insure that stable, reproducible data were collected. The sensor impedance response depends upon material composition and microstructure, molecular and electronic transport, as well as the following electrochemical reduction/oxidation reactions:

http://dx.doi.org/10.5772/62625

$$\frac{1}{2}O_2 + 2e^- \leftrightarrow O^{-2} \tag{6}$$

$$NO_2 + 2e^- \leftrightarrow NO + O^{-2} \tag{7}$$

The size of the electrolyte particles and degree of particle-to-particle connectivity influence the microstructure of the porous electrolyte, which affects gas and ionic transport pathways within the sensors. If gas transport through the porous microstructure or ionic transport through the particles is restricted, then reactions 6 and 7 will be impeded or limited. As shown in **Figure 1**, the electrolyte particle size and particle-to-particle connectivity increased with firing temperature, while the corresponding porosity decreased. Thus, it is necessary to establish a proper balance between gas and ionic transport pathways in order to promote NO_x sensitivity. The impedance data in **Figure 2** indicated a lower impedance resulted for sensors prepared at 1100°C, in comparison to the sensors prepared at 1000 and 1200°C. This result likely indicates that the microstructure of the sensors prepared at 1000°C lacked sufficient particle-to-particle connectivity, thereby limiting ionic transport and causing a larger impedance to be measured. On the other hand, the sensors prepared at 1200°C had more substantial particle-to-particle connectivity, but a lower porosity, which likely limited gas transport resulting in the higher impedance measurement. These data demonstrate the importance of understanding the behavior of gas and ionic transport pathways and their influence on optimizing sensor performance.

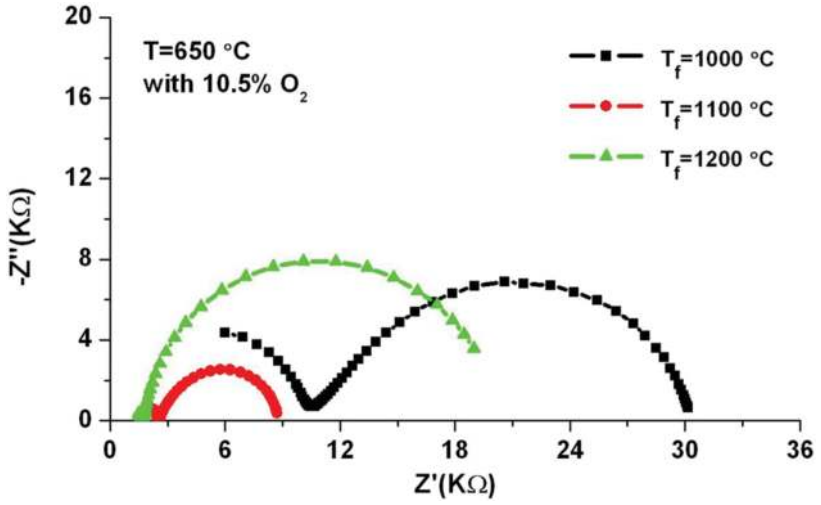

Figure 2. Nyquist plots of the sensors fired at 1000, 1100, and 1200°C while operating in 10.5% O_2 with N_2 as the balance.

To further analyze the electrical response of the sensors, equivalent circuit modeling with the Gamry EIS300 software was used to simulate the impedance measurements under various operating conditions. Bulk electrolyte properties associated with the porous YSZ microstructure, such as oxygen ion conductivity are described by the high-frequency arc (HFA) response. More importantly, the impedancemetric NO_x sensor response is primarily described by electrode reactions, which are presented by the low-frequency arc (LFA) response. The equivalent circuit model that best fits the sensor impedance results was $(R_1CPE_1)(R_2CPE_2)$, as shown in **Figure 3**.

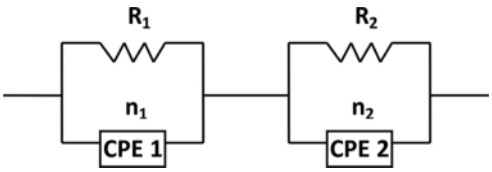

Figure 3. Equivalent circuit used to model the impedance data.

The resistor, R_1, was associated with the HFA and interpreted as the ionic transport resistance of the porous YSZ electrolyte. The HFA depends upon the porosity of the electrolyte as the porous microstructure creates tortuous pathways that can impede the flow of oxygen ions. The LFA resistance, R_2, described the interfacial resistance associated with TPB reactions. Such reactions include gas adsorption, dissociation, diffusion, and charge transfer. The equivalent circuit model accounted for the slight suppression of the arcs with constant phase elements, CPE_1 and CPE_2, which described the nonideal capacitance behavior of the electrolyte and electrodes, respectively. The CPE is defined by the following impedance equation:

$$Z(\omega) = \frac{1}{Y_0 (j\omega)^n} \tag{8}$$

where the impedance, Z, depends on the angular frequency, ω, and Y_0 is a constant. When $n = 1$, the $Z(\omega)$ represents a capacitance with a value equivalent to Y_0. Surface defects, interfacial reactions, as well as the morphology of the sensor components can cause the time constant for various reactions to differ resulting in nonideal capacitance behavior [8]. **Table 2** shows the simulated data generated for the sensors. These data were used to calculate the capacitance, C, associated with the high and low frequency sensor response according to the following equation:

$$C = \frac{\left[(R)(\mathrm{CPE})\right]^{\frac{1}{n}}}{R} \tag{9}$$

http://dx.doi.org/10.5772/62625

The CPE represents an ideal capacitor when $n = 1$. The n values shown in **Table 2** were relatively high, which indicated that the deviation from ideal capacitance behavior was small. Thus, the capacitance values determined from Eq (9) were reasonably accurate. The capacitance is associated with oxygen coverage at the Au/YSZ interface [9, 10]. The data in **Table 2** also show that the capacitance tended to decrease when NO was added to the test gas for sensors fabricated at temperatures up to 1100°C, which suggests that oxygen coverage diminished as NO occupied more sites along the TPB. The slight increase in capacitance observed in sensors prepared at 1150 and 1200°C may be related to the surface defects observed in these samples. Further discussion of the influence of oxygen on sensor behavior will be addressed in the later section of this chapter.

T_f (°C)	High-frequency arc		Low-frequency arc			
	10.5% O_2		10.5% O_2		10.5% O_2 + 100 ppm NO	
	Y1(F) 10^{-10}	n_1	Y2(F) 10^{-6}	n_2	Y2(F) 10^{-6}	n_2
950	0.638	0.89	0.427	0.77	0.416	0.77
1000	0.133	1.00	0.829	0.68	0.638	0.73
1050	1.149	0.86	0.923	0.79	0.909	0.79
1100	2.727	0.82	2.912	0.82	2.799	0.83
1150	2.550	0.83	1.867	0.92	1.871	0.92
1200	0.265	1.00	2.162	0.91	2.260	0.90

Table 2. Equivalent circuit fitting parameters are shown for sensor impedance data collected at 650°C.

NO_x sensitivity based on the impedancemetric method can be assessed using various parameters, including the angular phase response, magnitude of the impedance, and capacitance behavior. Here the angular phase response, θ, at specific frequencies, f, was used to measure NO sensitivity for the sensor with various porous electrolytes. The angular phase response is favored for yielding highly accurate data with limited noise contributions. An operating frequency of 40 Hz was determined from the impedance data to be a suitable frequency for monitoring the angular phase response of the sensors for various concentrations of NO, in order to achieve a relatively high sampling rate and response time. Based on the angular phase response, the sensitivity, $\Delta\theta/\theta$, of the sensors to NO was determined using the following equation: $\Delta\theta/\theta = [(\theta_{O2} - \theta_{NO})/\theta_{O2}]$. The term θ_{O2} corresponds to the baseline phase angle response when only O_2 was present, and θ_{NO} represents the phase angle response for a specific NO concentration. **Figure 4** shows the NO sensitivity gas experiments for the porous electrolyte sensors for operation at 650°C as the NO gas concentration was varied. The gas sensitivity data indicate that sensors prepared at 1050°C with an electrolyte porosity of 46% demonstrated greater NO sensitivity, particularly at lower concentrations of NO, in comparison to sensors fabricated at different temperatures. This suggests that the microstructure achieved at 1050°C promoted sufficient gas and ionic transport to enable reactions contributing to NO sensitivity to proceed more readily. It is important to note that although the gas experiments also indicated

reasonably high NO sensitivity responses by sensors fabricated at 950 and 1000°C, the higher firing temperature of 1050°C results in a stronger and more durable ceramic electrolyte. Thus, the microstructural and mechanical properties of electrolytes prepared at 1050°C contributed to greater gas sensitivity to NO along with greater sensor durability.

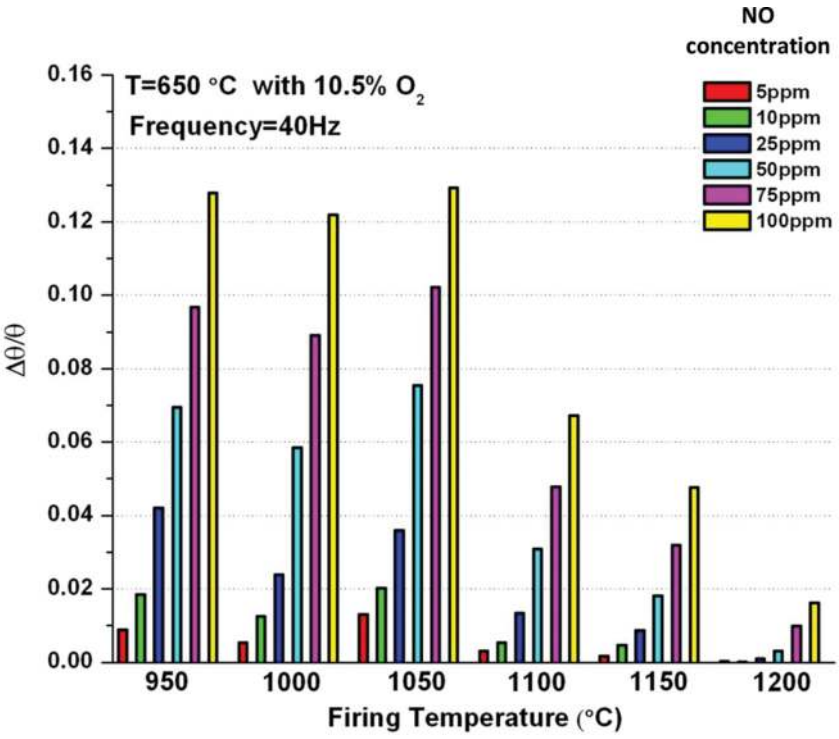

Figure 4. The fractional phase angle response for sensors fired at 950–1200°C in the presence of NO at a frequency of 40 Hz.

Knowledge of the oxygen and temperature dependence of the sensors can greatly aid interpretation of mechanisms and reaction kinetics governing NO sensing behavior. The oxygen partial pressure dependence was determined from the low-frequency arc, (R_1CPE_1) impedance data collected for each sensor. As shown in **Figure 5**, a power law dependence of $R_1 \propto (pO_2)^m$, where the slope m ≈ −0.47 to −0.72 was observed for the various porous electrolyte sensors. The slope values were found to become more negative as the microstructure of the electrolyte became less porous. Studies concerning oxygen partial pressure dependence have reported surface limiting reactions, such as dissociative adsorption or atomic oxygen as potential rate limiting mechanisms when the slope, m = −0.5 [11, 12]. Limited gas diffusion is commonly associated with slope values approaching −1. The observations of the data shown in **Figure 5** support gas diffusion becoming a rate limiting mechanism as the electrolyte porosity decreased

http://dx.doi.org/10.5772/62625

and the gas transport channels became more limited in the sensors prepared at higher firing temperatures. The sensors fabricated at 950–1050°C appeared to be limited by surface limiting processes. Since greater NO sensitivity was achieved for these sensors, it seems plausible that surface limiting processes do not significantly limit NO sensing behavior under the operating conditions tested.

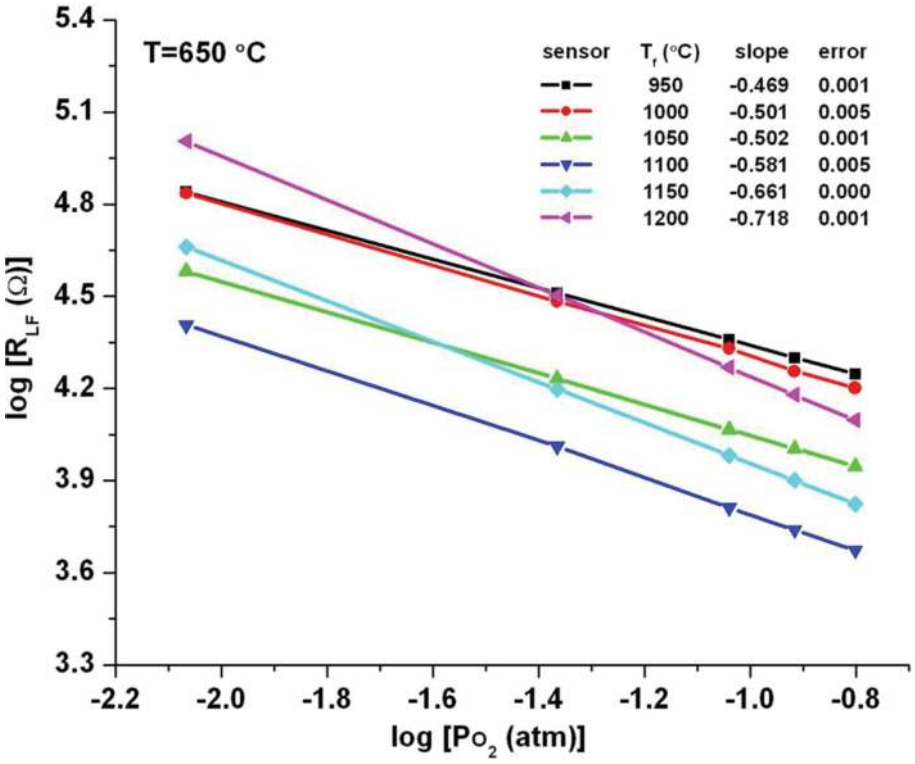

Figure 5. Oxygen partial pressure dependence of the various sensors at an operating temperature of 650°C under conditions where the oxygen concentration was varied from 1% to 18%.

The temperature dependence of the sensors was determined by the Arrhenius plots of the data that primarily described electronic/ionic transport behavior. From the slope of the plotted data, the activation energy, Ea, was determined for each sensor. The data in **Figure 6** indicated that oxygen ions were able to travel more readily as the operating temperature increased; and, that greater ionic transport was achieved as the porosity of the sensor electrolyte decreased. Sensors with lower porosity had larger YSZ particles and greater particle-to-particle connectivity, which supported greater ionic transport. The activation energy values presented here were typical for porous YSZ electrolyte NO_x sensors with Au electrodes. The activation energy data in **Figure 6**, taken into consideration with the NO sensitivity data in **Figure 4**, suggest that sufficiently high oxygen ion transport activity can limit NO sensitivity. Thus, a microstructure

that creates a suitable balance between the gas and ionic transport pathways is necessary for establishing optimal NO_x sensing properties.

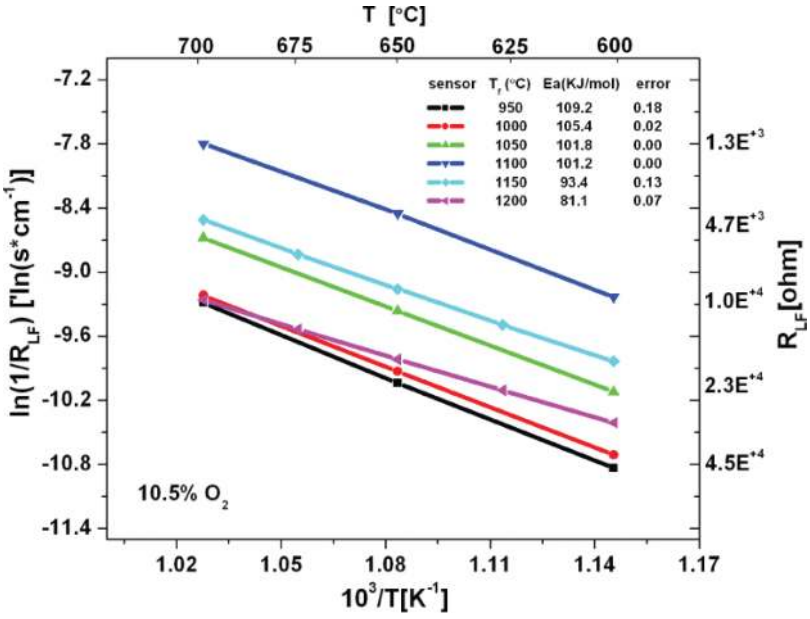

Figure 6. The temperature dependence is described by the Arrhenius plot for the sensors fired at 950–1200°C along with corresponding activation energies.

6. Conclusions

Porous electrolyte-based NO_x exhaust gas sensors are a novel and promising concept for expanding the capabilities of automotive gas sensing technology. The work presented here using the impedancemetric method clearly demonstrated the influence of the porous electrolyte microstructure on NO_x sensing behavior. Substantial differences in the impedance response, sensitivity, rate limiting mechanisms, and activation energies were observed in the data collected for NO_x sensors with porous electrolytes ranging from 50% to 44%. The increase in NO_x sensitivity observed in the sensors fabricated at 1050°C with a corresponding electrolyte porosity of 46% was promoted by establishing a microstructure that provided a proper balance between the gas transport pathways created by the porous microstructure and the ionic transport pathways formed by the YSZ particles. In addition, the resulting particle size and particle-to-particle contact of sensors with an electrolyte fabricated at 1050°C formed an electrolyte/electrode/gas interface (i.e., TPB) that enabled reactions favoring NO_x to proceed more readily. The phase angle measurements collected at 40 Hz indicated NO_x sensitivity can be achieved at significantly low concentrations (e.g., 5 ppm), which suggests that rapid sensing

http://dx.doi.org/10.5772/62625

is feasible for such sensors. Within the range of porosities tested, surface limiting reactions appeared to be a rate limiting mechanism based on the oxygen partial pressure dependence. However, this limiting mechanism did not appear to significantly impede NO_x sensing capabilities for sensors prepared at 1050°C. A strong relationship was observed between the sensor electrolyte porosity and the sensor activation energy. Lower activation energies correlated with lower electrolyte porosity. As research continues, the outcomes are expected to contribute to a more complete understanding of NO_x sensor behavior and provide fundamental knowledge necessary for the advancement of NO_x exhaust gas sensor technology.

Acknowledgements

The authors thank Dr. Weizhong Dai and Dr. Fei Han for carrying out the mathematical calculations used to determine the porosity of the electrolyte-based NO_x sensors. The authors also extend their appreciation to Mr. Robert Novak and Dr. Jaco Visser of Ford Motor Company for providing technical support and meaningful discussions that contributed to this work. Funding of this work was provided by the National Science Foundation under the Ceramics Program (DMR-1410670).

Author details

Erica Perry Murray* and Ling Cui

*Address all correspondence to: emurray@latech.edu

Institute for Micromanufacturing, Louisiana Tech University, Ruston

References

[1] Bandivadekar A, Bodek K, Cheah L, Evans C, Groode T, Heywood H, Kasseris E, Kromer M, Weiss M. On the Road in 2035: Reducing Transportation's Petroleum Consumption and GHG Emissions. MIT Laboratory for Energy and the Environment, Cambridge, MA, Report No. LFEE 2008-5 RP, July 2008.

[2] United States Environmental Protection Agency, 2007 Progress Report: Vehicle and Engine Compliance Activities, EPA-420-R-10-022, Aug 2010.

[3] United States Environmental Protection Agency, EPA's Program for Cleaner Vehicles and Cleaner Gasoline, EPA420-F-99-051, Dec 1999.

[4] Martin L, Woo L, Glass R. Impedancemetric NO_x sensing using YSZ electrolyte and YSZ/Cr_2O_3 composite electrodes. Journal of the Electrochemical Society. 2007; 154(3):J97-J104, doi:10.1149/1.2430646.

[5] Ling C, Fei H, Weizhong D, Erica PM. Influence of microstructure on the sensing behavior of NO_x exhaust gas sensors. Journal of the Electrochemical Society. 2014; 161(3):B34-B38, doi:10.1149/2.088403jes.

[6] Jan VH, Augustin JM, Thampi KR. Conductivity measurements of various Yttria-stabilized zirconia samples. Journal of Materials Science. 1994; 29(14):3691–3701, doi: 10.1007/BF00357336.

[7] Praveen KS, Eric LB, Rangachary M, Mark AN, Dennis T, Fernando HG. Effect of yttria-stabilized zirconia sintering temperature on mixed potential sensor performance. Solid State Ionics. 2010; 181(19):947–953.

[8] Evgenij B, Ross M. Impedance spectroscopy theory, experiment, and applications. New Jersey: John Wiley & Sons, Inc., 2005.

[9] Ling C, Erica PM. Effect of electrode configuration on nitric oxide gas sensor behavior. Sensors. 2015; 15:24573–24584. doi: 10.3390/s150924573.

[10] Woo L, Martin L, Robert SG, Wensheng W, Sukwon J, Raymond JG, Erica PM, Rober FN, Jaco HV. Effect of electrode composition and microstructure on impedance metric nitric oxide sensors based on YSZ electrolyte. Journal of the Electrochemical Society. 2008; 155(1):J32-J40, doi:10.1149/1.2804766.

[11] Takeda Y, Kanno R, Noda M, Tomida Y, Yamamoto O. Cathodic Polarization phenomena of perovoskite oxide electrodes with stabilized zirconia. Journal of the Electrochemical Society. 1987; 134(11):2656–2661, doi:10.1149/1.2100267.

[12] Fukunaga H, Koyama M, Takahashi N, Wen C, Yamada K. Reaction model of dense $Sm_{0.5}Sr_{0.5}CoO_3$ as SOFC cathode. Solid State Ionics. 2000; 132:279–285.